Discoveries

ORIGINAL RESEARCH COMMUNICATION

Menadione-Induced DNA Damage Leads to Mitochondrial Dysfunction and Fragmentation During Rosette Formation in Fuchs Endothelial Corneal Dystrophy

Adna Halilovic,[1] Thore Schmedt,[1] Anne-Sophie Benischke,[1] Cecily Hamill,[1] Yuming Chen,[1] Janine Hertzog Santos,[2,*] and Ula V. Jurkunas[1]

Abstract

Aims: Fuchs endothelial corneal dystrophy (FECD), a leading cause of age-related corneal edema requiring transplantation, is characterized by rosette formation of corneal endothelium with ensuing apoptosis. We sought to determine whether excess of mitochondrial reactive oxygen species leads to chronic accumulation of oxidative DNA damage and mitochondrial dysfunction, instigating cell death. *Results:* We modeled the pathognomonic rosette formation of postmitotic corneal cells by increasing endogenous cellular oxidative stress with menadione (MN) and performed a temporal analysis of its effect in normal (HCEnC, HCECi) and FECD (FECDi) cells and *ex vivo* specimens. FECDi and FECD *ex vivo* specimens exhibited extensive mtDNA and nDNA damage as detected by quantitative PCR. Exposure to MN triggered an increase in mitochondrial superoxide levels and led to mtDNA and nDNA damage, while DNA amplification was restored with NAC pretreatment. Furthermore, MN exposure led to a decrease in $\Delta \Psi m$ and adenosine triphosphate levels in normal cells, while FECDi exhibited mitochondrial dysfunction at baseline. Mitochondrial fragmentation and cytochrome *c* release were detected in FECD tissue and after MN treatment of HCEnCs. Furthermore, cleavage of caspase-9 and caspase-3 followed MN-induced cytochrome *c* release in HCEnCs. *Innovation:* This study provides the first line of evidence that accumulation of oxidative DNA damage leads to rosette formation, loss of functionally intact mitochondria *via* fragmentation, and subsequent cell death during postmitotic cell degeneration of ocular tissue. *Conclusion:* MN induced rosette formation, along with mtDNA and nDNA damage, mitochondrial dysfunction, and fragmentation, leading to activation of the intrinsic apoptosis *via* caspase cleavage and cytochrome *c* release. *Antioxid. Redox Signal.* 24, 1072–1083.

Introduction

HUMAN CORNEAL ENDOTHELIAL CELLS (HCEnCs) are a monolayer of neural crest-derived hexagonal cells situated in the posterior surface of the cornea and have a key function of maintaining appropriate corneal hydration that is compatible with clear vision. HCEnCs are arrested in the postmitotic state and do not proliferate *in vivo* (3, 38, 46). Fuchs endothelial corneal dystrophy (FECD) leads to gradual and age-related loss of HCEnCs and leads to corneal edema and blindness (27, 46). FECD affects

upto 4% of the U.S. population over the age of 40 and is the leading indication for endothelial keratoplasty in the United States (9, 32). Morphologically, the key characteristics of FECD are the disruption of the endothelial cell mosaic by deposition of guttae, the extracellular matrix deposits, and concurrent endothelial cell loss that form a ring or rosette around the bases of guttae (41). The detection of rosettes in whole mounts of FECD specimens has been a prominent feature in the previous studies that implicated oxidative stress in the pathogenesis of FECD (2, 22–25, 47).

[1]Department of Ophthalmology, Schepens Eye Research Institute, Massachusetts Eye and Ear Infirmary (MEEI), Harvard Medical School, Boston, Massachusetts.
[2]Department of Pharmacology and Physiology, New Jersey Medical School Rutgers, Rutgers University, New Jersey.
*Current affiliation: Epigenetics and Stem Cell Biology Laboratory, National Institute of Environmental Health Sciences (NIEHS), Research Triangle Park, North Carolina.

Innovation

This study provides the first line of evidence revealing amplified accumulation of oxidative DNA damage and mitochondrial fragmentation in the *in vitro* and *ex vivo* Fuchs endothelial corneal dystrophy (FECD) corneal endothelium. We have shown that menadione induced oxidative stress, leading to rosette formation, DNA damage, and subsequent induction of endothelial cell death corresponding to findings in an *ex vivo* FECD specimen.

Specifically, studies on the composition of rosettes showed overproduction of clusterin (CLU) and transforming growth factor-β-induced (TGFBI) protein, as well as increased proportion of TUNEL-positive cells adjacent to the acellular centers of the rosettes (2, 22, 23). Evidence indicated an underlying oxidant–antioxidant imbalance, which leads to oxidant-induced apoptosis, in FECD *ex vivo* and *in vitro* models (2, 23). Nevertheless, the mechanism leading to HCEnC degeneration is not known. Postmitotic cells of the ocular tissues, such as HCEnCs, have a lifelong exposure to ultraviolet light and exuberant metabolic activity due to pumping of ions; therefore, due to limited regenerative capacity and division, HCEnCs are susceptible to oxidized DNA accumulation over time (29). To study the role of DNA damage in the FECD pathogenesis, we developed an *in vitro* model by inducing intracellular stress seen in the cells surrounding the rosettes and mimicking the oxidant–antioxidant imbalance seen in FECD.

Our previous studies detected higher levels of 8-hydroxy-2′-deoxyguanosine (8-OHdG) and increased levels of intracellular reactive oxygen species (ROS) and apoptosis in FECD corneal endothelium (23). Since only 10% of ROS-induced DNA damage is captured by the 8-OHdG assay, and our previous work did not distinguish between mtDNA and nDNA damage, we utilized a quantitative PCR methodology to distinguish genomic damage in normal and FECD cell lines and tissue specimens. The aim of this study was to determine whether nDNA and/or mtDNA damage is involved in the pathogenesis of FECD. We formulated the hypothesis that chronic accumulation of oxidative DNA damage in HCEnCs leads to mitochondrial dysfunction and apoptosis seen in FECD. The biological consequence of DNA damage, mainly mtDNA, has been linked to multiple oxidative stress-induced degenerative disorders, including Alzheimer's and Parkinson's diseases (8, 17) and age-related macular degeneration. However, the integrity of the DNA has not been studied in depth in corneal endothelium and FECD.

To understand the basis of ROS-induced damage in FECD corneal endothelium, we increased intracellular ROS by treating cells with menadione (MN), testing its effects in normal and FECD cells. MN is a quinone that is metabolized by a 1-electron reducing enzyme, such as NADPH-cytochrome P450 reductase or mitochondrial NADH-ubiquinone oxidoreductase, and generates intracellular superoxide and an unstable semiquinone radical that in turn increases intracellular ROS (Fig. 1A). In this study, we analyzed the influence of MN exposure on normal HCEnC morphology and detected that mitochondrial ROS generation led to rosette formation in normal HCEnCs, mimicking the changes seen in the *ex vivo* FECD specimens. These findings led us to develop an *in vitro* model, which analyzes the direct influence of intracellular

ROS generation on DNA lesion levels, mitochondrial distribution, and the inner mitochondrial membrane potential ($\Delta\Psi$m) during rosette formation. As corneal endothelium is especially rich in mitochondria, mtDNA damage and cell dysfunction could be the basis of decline in local adenosine triphosphate (ATP) supply, leading to cellular apoptosis in FECD (43). We detected that superoxide generation by MN induced DNA damage and led to the disruption of the $\Delta\Psi$m, leading to the loss of functionally intact mitochondria. DNA-damaging influence of MN led to mitochondrial fragmentation and activation of apoptosis in corneal endothelium. Taken together, these findings demonstrate a novel pathogenic mechanism in which DNA damage and subsequent mitochondrial fragmentation lead to postmitotic cell loss in the ocular tissue.

Results

MN induces rosette formation in HCEnCs—the hallmark of FECD

To investigate the effects of intrinsic oxidative stress on corneal endothelium, MN was used in our study. MN is metabolized by a one-electron reduction, generating superoxide and unstable semiquinone, and inducing intracellular oxidative stress (Fig. 1A) (30). Normal telomerase-immortalized human corneal endothelial (HCEnC-21T) cells were grown in hexagonal monolayers and exposed to MN to determine its effects on cellular viability and morphology. Cellular viability, determined by trypan blue dye exclusion, was not significantly reduced due to increasing doses (25, 50, and 100 μM) of MN for 1 h. MN decreased viable cell numbers at 50 μM (by 21%, $p < 0.001$) and 100 μM (by 39%, $p < 0.001$), starting with a 2-h exposure; the viability continued to decline after the 4-h MN treatment with cell viability falling by 41% ($p < 0.001$) and 49% ($p < 0.001$), respectively (Fig. 1B). Cell morphology revealed that after MN treatment, cell monolayers developed rosette-like clusters with clear acellular centers and spindle-like cells surrounding them. The centers often exhibited a dying or a detaching cell with surrounding cell processes extending toward the detaching cells (Fig. 1G–I). Rosette-like structures formed as early as 1 h after 50 μM MN exposure (Fig. 1G) and increased in number and size with increased incubation time (Fig. 1H, I) and MN dose (Supplementary Fig. S1; Supplementary Data are available online at www.liebertpub.com/ars). With longer incubation times, the rosettes increased in size with increased stretching of the cell processes around the perimeter of the acellular spaces (Fig. 1I). Rosette formations were identical to the ones detected in *ex vivo* corneal endothelial specimens taken from FECD patients (Fig. 1E, F) (24). This unique morphological feature was not observed in HCEnCs grown in the basal medium for 4 h (Supplementary Fig. S1) or when exposed to staurosporine (STS), a proapoptotic agent (Fig. 1C). In addition, MN-induced rosettes exhibited enhanced CLU immunofluorescence, similarly to findings seen in *ex vivo* FECD specimens (Fig. 1F, J). Moreover, the relative expression of *CLU* and *TGFBI* gradually increased during the rosette formation, indicating *in vitro* deposition of secretory and extracellular matrix proteins seen in FECD (Supplementary Fig. S2A).

To represent chronic endothelial dysfunction seen in FECD, low-dose MN (1 and 10 μM) exposure for 24 and 48 h was performed. Chronic stress induced rosette formation in a
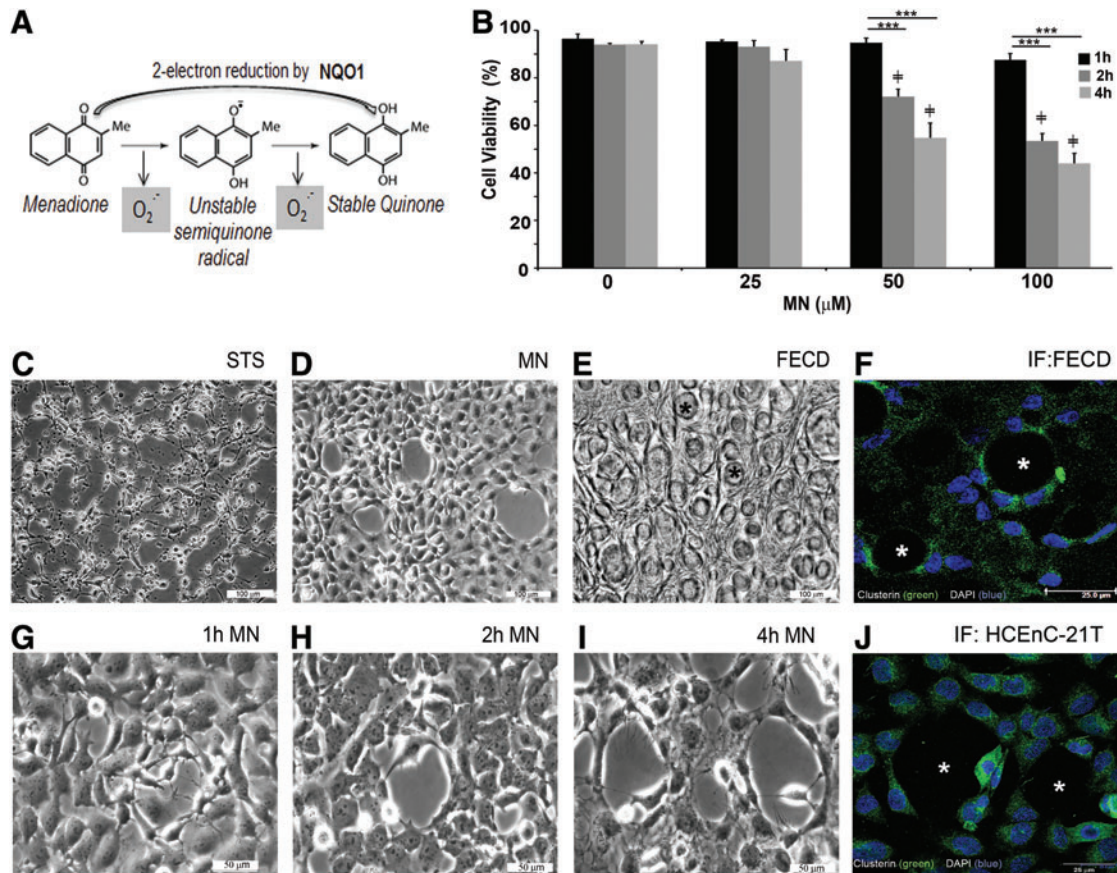
FIG. 1.   **MN induced rosette formation in immortalized corneal endothelial cells. (A)** Schematic representation of MN degradation into a stable quinone in the presence of NQO1. HCEnC-21T cells were treated with various doses of MN and cellular viability was analyzed at 0, 1, 2, and 4-h time points. **(B)** Cellular viability of MN-treated HCEnC-21T cells in a time and dose–response analysis using trypan *blue* dye exclusion assay. Phase-contrast images were captured of HCEnC-21T cells treated with **(C)** STS, 4 h **(D)** 50 μM MN, showing rosette formation at 4 h. **(E)** cellular morphology of a postkeratoplasty human FECD specimen (47 male, * guttae). **(F)** Immunofluorescence image of clusterin staining around guttae (*) in an FECD specimen (74 female) and **(J)** around rosette-like formation in HCEnCs. Captured images of rosette formation at different time intervals, starting at **(G)** 1 h, **(H)** 2 h, and **(I)** 4 h after 50 μM MN treatment. Data are expressed as the mean $\pm$ SE ($n = 6$). Two-way ANOVA applied for statistical significance comparing treated samples (2, 4 h) *versus* 1 h (*$p < 0.05$, ***$p < 0.001$) and 25, 50, 100 μM treated *versus* control, 0 ($\neq p < 0.0001$). FECD, Fuchs endothelial corneal dystrophy; HCEnC, human corneal endothelial cell; MN, menadione; NQO1; NAD(P)H quinone dehydrogenase 1; STS, staurosporine. To see this illustration in color, the reader is referred to the web version of this article at www.liebertpub.com/ars

time-dependent manner (Supplementary Fig. S3), similarly to what was detected after 50 μM MN exposure (Fig. 1). Moreover, *CLU* and *TGFBI* mRNA levels were upregulated after 48 h with 10 μM MN treatment (Supplementary Fig. S2B), similarly to what was seen after more acute exposure to MN (Supplementary Fig. S2A) and in *ex vivo* specimens (22, 24). Since more acute MN exposure accelerated changes in the endothelial cell morphology and extracellular protein composition seen after chronic exposure (Supplementary Figs. S2 and S3), we induced the rosette formation with ensuing macromolecular damage with the acute stress model.

mtDNA and nDNA damage in FECD

Our hypothesis was that accumulation of oxidative DNA damage contributes to endothelial cell degeneration in FECD. To test this, we assessed MN-induced DNA damage in normal corneal endothelial cells during rosette formation.

As the optimal rosette formation without significant decline in cell viability (79% live cells) occurred after 2 h of treatment with 50 μM MN, we exposed cells to this sublethal dose of MN. Long-extension PCR was performed to investigate mtDNA and nDNA damage separately (37). The relative amplification of mtDNA short fragments served as an estimate of mtDNA copy number as the probability of inducing DNA damage in a short fragment was low (Fig. 2A). Small mtDNA amplification was not altered with MN or NAC treatment in the normal (HCEnC-21T or HCECi) or FECDi cell lines. However, mitochondrial copy number by LX-PCR was 80% ($p < 0.001$) lower in FECDi cells compared with normal cells at baseline and remained at a reduced level after MN exposure, indicating that FECDi cells have significantly lower quantity of mitochondria compared with normal cells.

In normal endothelial cell lines (HCEnC-21T and HCECi), a low dose of MN, 25 μM, did not have an effect on mtDNA damage compared with untreated control, while 50 μM MN
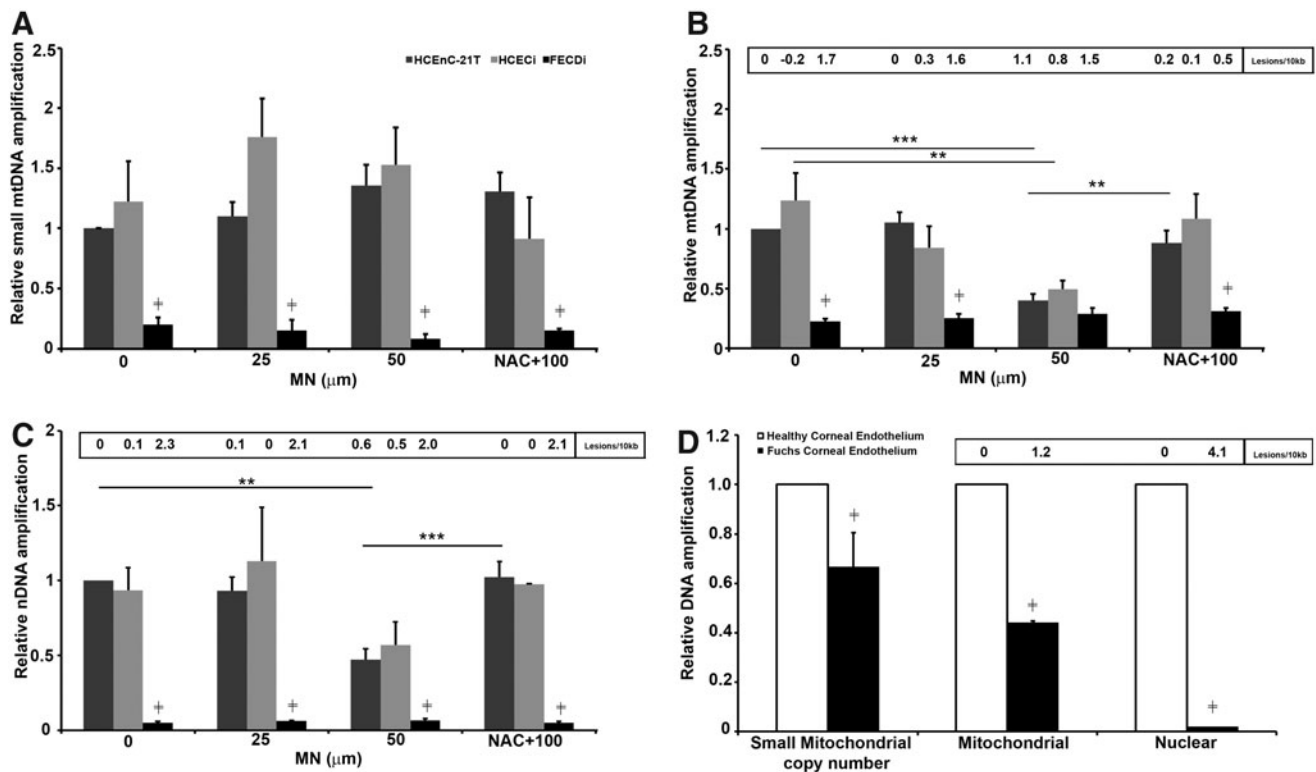
FIG. 2. **Mitochondrial and nuclear DNA damage in FECD**. All three cell lines were treated with 25 μM or 50 μM MN for 2 h or pretreated with NAC in the presence of 100 μM MN for 2 h and assessed for DNA damage using long-amplicon qPCR. Control (0) included DMEM for 2 h. Data represented in **(A)** DNA amplification of the small mitochondrial amplicon (250 bp), **(B)** DNA amplification and lesion frequency of mitochondrial target amplicon (8.9 kb), and **(C)** DNA amplification and lesion frequency of β-globin (nuclear) target amplicon (13.5 kb) ($n = 3$). Relative amplification was calculated comparing treated samples with untreated HCEnC-21T cells. Panel **(D)** depicts DNA amplification and lesion frequency in pooled normal ($n = 22$ for mtDNA and $n = 15$ for nDNA) and FECD ($n = 31$ for mtDNA and $n = 11$ for nDNA) specimens. Data are expressed as the mean ± SE. Two-way ANOVA was applied for statistical significance comparing treated samples with untreated control (0). (**$p < 0.01$, ***$p < 0.001$, $p \neq < 0.01$ FECDi/FECD *vs.* normal cells [HCEnC-21T, HCECi] or normal donor corneal endothelium). mtDNA, mitochondrial DNA; NAC, N-acetyl-cysteine.

decreased DNA amplification by 60% and 50% and increased lesion frequency to 1.1 ($p < 0.001$) and 0.8 in HCEnC-21T and HCECi cells, respectively (Fig. 2B). DNA damage did not further decrease with 100 μM MN (data not shown) compared with 50 μM. Pretreatment with NAC significantly increased DNA amplification, suggesting that MN-induced DNA damage was mediated by ROS. At baseline, FECDi exhibited significantly higher mtDNA lesion frequency (1.7 lesions/kb, $p < 0.001$) than HCEnC-21T (0 lesions/10 kb) and HCECi (−0.2 lesions/10 kb) cells, respectively. MN did not further induce DNA damage in FECDi as the lesion number remained around 1.7–1.5 lesions/10 kb with or without MN.

Interestingly, we also detected a marked decrease in nDNA amplification by 95% ($p < 0.001$) and an increase in lesion number to 2.3 in FECDi at baseline compared with normal cell lines. The higher nDNA lesion frequency persisted in FECDi with MN treatments and NAC rescue (Fig. 2C). MN treatment did not induce any further damage in FECDi cells. Long-extension PCR detected a 53% and 43% decrease in DNA amplification of the β-globin gene and increase in lesion number to 0.6 and 0.5 with 50 μM MN in HCEnC-21T and HCECi cells, respectively. Pretreatment with NAC rescued the effect of MN (data not shown) back to control level (untreated) in HCEnC-21T and HCECi cells.

To corroborate the cell line data, FECD specimens were collected for DNA integrity analysis; samples were pooled due to low amount of cells retrieved. The mtDNA and nDNA damage in FECD was compared with age-matched normal cornea donors (Fig. 2D). FECD specimens exhibited a 37% lower small mitochondrial copy number ($p < 0.01$) compared with normal specimens. Moreover, when compared with normal specimens, FECD mtDNA showed a marked reduction in amplification (by 56%; $p < 0.001$), corresponding to 1.2 lesions/kb. Furthermore, FECD nDNA amplification was significantly lower (99%; $p < 0.001$) corresponding to 4.1 lesions/kb compared with normal corneal donors. These data indicate a greater accumulation of basal mtDNA and nDNA damage in FECD than what is seen in normal aging of corneal endothelium.

*MN induced mitochondrial oxidative stress
and dysfunction as seen in FECD*

Next, we sought to determine whether DNA damage leads to mitochondrial ROS accumulation and mitochondrial dysfunction. We analyzed the influence of MN exposure on mitochondrial ROS generation and cellular ability to maintain $\Delta\Psi m$ in a dose- and time-dependent manner. As mitochondrial

dysfunction can be the basis of cellular death during rosette formation, we investigated whether ATP production was altered during the process.

MN has been shown to increase mitochondrial-derived ROS (30). Thus, we determined mitochondrial superoxide levels by MitoSOX™ Red, a mitochondrial superoxide indicator, using flow cytometry (Fig. 3A). FECDi cells had significantly higher mitochondrial superoxide levels (by 22%, $p < 0.01$) at baseline compared with HCECi cells, consistent with the basal mtDNA damage. Mitochondrial superoxide levels increased eightfold with 25 μM MN compared with

baseline in HCEnC-21T and HCECi cells, respectively. Furthermore, 50 μM MN increased superoxide levels up to 10–12-fold in normal cells from baseline and no further significant increase was observed with 100 μM MN (Fig. 3B). Superoxide generation was abrogated by cotreatment of cells with NAC compared with 100 μM MN treatment alone in normal cell lines, but not in FECDi, potentially indicating greater baseline oxidant–antioxidant imbalance of the diseased cells.

The integrity of $\Delta \Psi$m was measured by the JC-1 assay. Cells were treated with different MN concentrations and
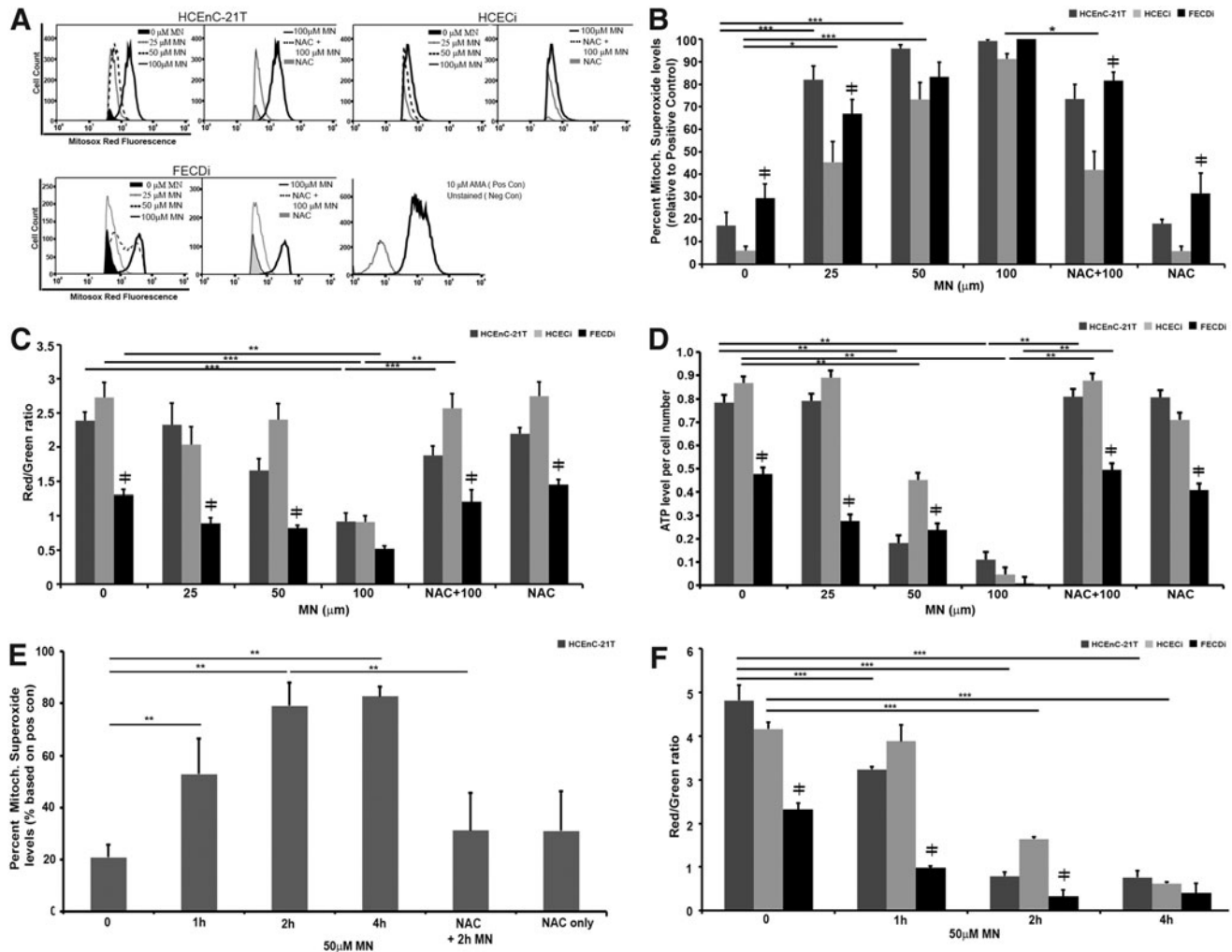
FIG. 3.   MN induced mitochondrial dysfunction. HCEnC, HCECi, and FECDi cells were exposed to MN in a dose-dependent manner for 1 h with or without NAC pretreatment and collected for measurement of mitochondrial ROS production by flow cytometry, ATP levels, and $\Delta \Psi$m using the JC-1 assay, as described in the Materials and Methods section. **(A)** Flow cytometry analysis of mitochondrial $O_2^{\bullet-}$ production was measured by MitoSox *Red* fluorescence intensity and represented by histograms. MN increased MitoSOX *Red* intensity as early as 25 μM, while NAC pretreatment attenuated 100 μm MN-induced MitoSox *Red* intensity ($n = 3$); **(B)** Quantification of flow cytometry data. Results were normalized to the positive control, antimycin A-treated cells. ($n = 3$); **(C)** ATP levels were measured by a luminescence assay and normalized to cell number per sample ($n = 6$ in duplicate); **(D)** Represents $\Delta \Psi$m levels as a ratio of *red/green* fluorescence, which is a change in JC-1 properties from aggregate to monomeric form in MN-treated cells ($n = 4$ in duplicate); **(E)** Time course analysis of mitochondrial $O_2^{\bullet-}$ levels with 50 μM MN in HCEnC-21T cells with or without NAC pretreatment ($n = 4$ in duplicate); **(F)** Time course analysis of MMP levels with 50 μM MN in all three cell lines ($n = 4$ in duplicate). Data are expressed as the mean $\pm$ SE. Two-way ANOVA was applied for statistical significance, comparing treated samples with untreated control (0). *$p < 0.05$, **$p < 0.01$, ***$p < 0.001$, $\neq p < 0.05$ FECDi *versus* HCEnC-21T and/or HCECi. ATP, adenosine triphosphate.

analyzed after 1 h (Fig. 3C). At baseline, $\Delta\Psi$m was lower by 52% ($p < 0.001$) and 45% ($p < 0.001$) in FECDi compared with HCEnC-21T and HCECi cells, respectively. FECDi continuously exhibited lower $\Delta\Psi$m with 25 and 50 μM MN compared with normal cells. Normal cells were resistant to changes in the $\Delta\Psi$m up until 100 μM MN, where $\Delta\Psi$m decreased by 66% ($p < 0.001$) and 61% ($p < 0.001$) in HCEnC-21T and HCECi cells, respectively. Pretreatment with NAC restored $\Delta\Psi$m levels back to baseline in all three cell lines, suggesting that the effect of MN on $\Delta\Psi$m was ROS mediated.

To determine whether MN-induced mitochondrial impairment leads to depletion of ATP, we determined ATP levels based on the conversion of the D-luciferin to the luminescent product in the presence of ATP (Fig. 3D). FECDi exhibited greater susceptibility to MN-induced ATP loss compared with normal cells. At baseline, FECDi has lower ATP production by 39% ($p < 0.001$) and 45% ($p < 0.001$) compared with HCEnC-21T and HCECi cells, respectively. Even with a low dose of MN (25 μM), ATP levels decreased in FECDi by 42% ($p < 0.05$) from baseline, but did not significantly change in normal cells. Normal cells responded to higher doses of MN by lowering ATP production by 77% ($p < 0.001$) and 48% ($p < 0.001$) in HCEnC-21T and HCECi cells, respectively, after 50 μM MN and to almost undetectable levels after 100 μM MN. Pretreatment with NAC restored ATP back to control levels. In summary, increased doses of MN induced mitochondrial depolarization and loss of ATP in normal cells to the levels seen in FECDi. Pretreatment with NAC protected $\Delta\Psi$m depolarization and ATP loss from MN-induced oxidative stress.

While we observed a dose-dependent increase in superoxide levels and loss of ATP and $\Delta\Psi$m due to MN, the optimal dose for rosette formation without significant cell loss was seen at 50 μM dose. Therefore, to investigate temporal mitochondrial involvement during rosette formation, a time course analysis of superoxide and $\Delta\Psi$m with 50 μM MN was performed. Mitochondrial superoxide levels significantly increased starting at 1 h of treatment, corresponding with the start of rosette formation (Figs. 3E and 1G). Superoxide levels continued to escalate at 2 h and plateaued at 4 h, corresponding with the increase in cell death associated with progressive rosette formation (Fig. 1B, I). Conversely, $\Delta\Psi$m levels decreased after 2 h of MN treatment, correlating with the time point of greatest level of DNA damage in both normal cell lines (Figs. 2B, C, and 3F). Our data indicate that during rosette formation, MN increased mitochondrial ROS production after 1 h of treatment leading to the eventual decrease of $\Delta\Psi$m at 2 h. MN induced mitochondrial depolarization up to the level of FECDi at the 4-h time point (Fig. 3F).

MN induces mitochondrial fragmentation and cytochrome c release seen in FECD

Considering that mitochondrial morphology has been shown to be regulated by $\Delta\Psi$m (18), and we detected a loss of $\Delta\Psi$m in FECDi and in MN-treated normal cells, we next sought to investigate whether mitochondrial integrity and morphology were compromised during rosette formation. Studies have shown that depletion of ATP and the alteration in $\Delta\Psi$m trigger general fragmentation of the mitochondria (42). Mitochondrial morphology of HCEnC-21T cells was

assessed by confocal microscopy with immunostaining of cytochrome c to visualize mitochondria after cells were treated with 50 μM MN for 0, 1, 2, 4, and 6 h (Fig. 4A, left panel). This method enabled visualization of mitochondrial distribution during rosette formation in a time-dependent manner. Normal endothelial cells (HCEnC-21T) and *ex vivo* specimens displayed elongated tubular mitochondrial networks, which readily stained with intracellular cytochrome c (Fig. 4A, left side and B, bottom image). The 1-h treatment of MN did not affect the overall organization of the mitochondrial network compared with the control. After 2 h of MN treatment, the mitochondria started to lose their tubular shape and mitochondria became fragmented compared with the untreated control. There was an increase in spherical mitochondria at the 4-h time point. With increasing doses of MN, mitochondria shape changed into small and spherical organelles and tended to aggregate around the nuclei. Similar changes were seen with rotenone, a known inhibitor of complex I of the electron transport chain and inducer of mitochondrial fragmentation (Supplementary Fig. S4A) (10). At 6 h, MN induced abnormal mitochondrial clustering and cytochrome c release, indicative of excessive fragmentation and cell death. Since it is known that (during the early stage of apoptosis) several proteins such as cytochrome c are released from the mitochondrial intermembrane space to the cytosol (39), we monitored cytochrome c release after treatment with MN. HCEnC-21T cells were pretreated with pan-caspase inhibitor, zVAD-fmk, followed by 50 μM MN for 0, 1, 2, 4, and 6 h (Fig. 4A, right panel), and stained using cytochrome c. Similarly, we found that with MN treatment, there was a transition from the typical tubular mitochondrial network of healthy cells (control and 1 h MN) into vesicular punctiform mitochondria (2 and 4 h). The intracytoplasmic staining with cytochrome c was first detected after the 4-h treatment in cells mostly surrounding rosettes (Fig. 4, asterisk). However, even at the 4-h time point, some cytochrome c was still retained in mitochondria, indicating that only a portion of cells were undergoing apoptosis. The cells with most cytochrome c release were located next to rosettes. With prolonged MN treatment (6 h), cytochrome c was released diffusely and completely into the cytosol. Low-magnification images revealed widespread formation of rosettes and generalized release of cytochrome c (Supplementary Fig. S4B). These findings indicate that mitochondrial fragmentation occurred at an early stage of cellular apoptosis and eventually led to cytochrome c release during rosette formation. Similarly, application of STS led to cytochrome c release and served as a positive control for apoptosis (Supplementary Fig. S4A) (11). To determine whether mitochondrial morphology is altered in FECD pathogenesis, postkeratoplasty FECD tissues were stained for the mitochondrial marker cytochrome c (4, 7, 10, 31). In the FECD male specimen (Fig. 4B, upper images), we detected cytochrome c release, predominantly expressed around cells adjacent to the guttae, which were stained with DAPI. We also found that mitochondria showed a stretched appearance with their long axis directed toward the guttae (Fig. 4B, upper images). In the FECD female specimen (Fig. 4B, lower image), mitochondria were fragmented and appeared as round and smaller in size. As the guttae get bigger than the endothelial cell in size, adjacent cells seem to form a rosette, corresponding to our *in vitro* model with MN exposure (Fig. 1D, G–J).
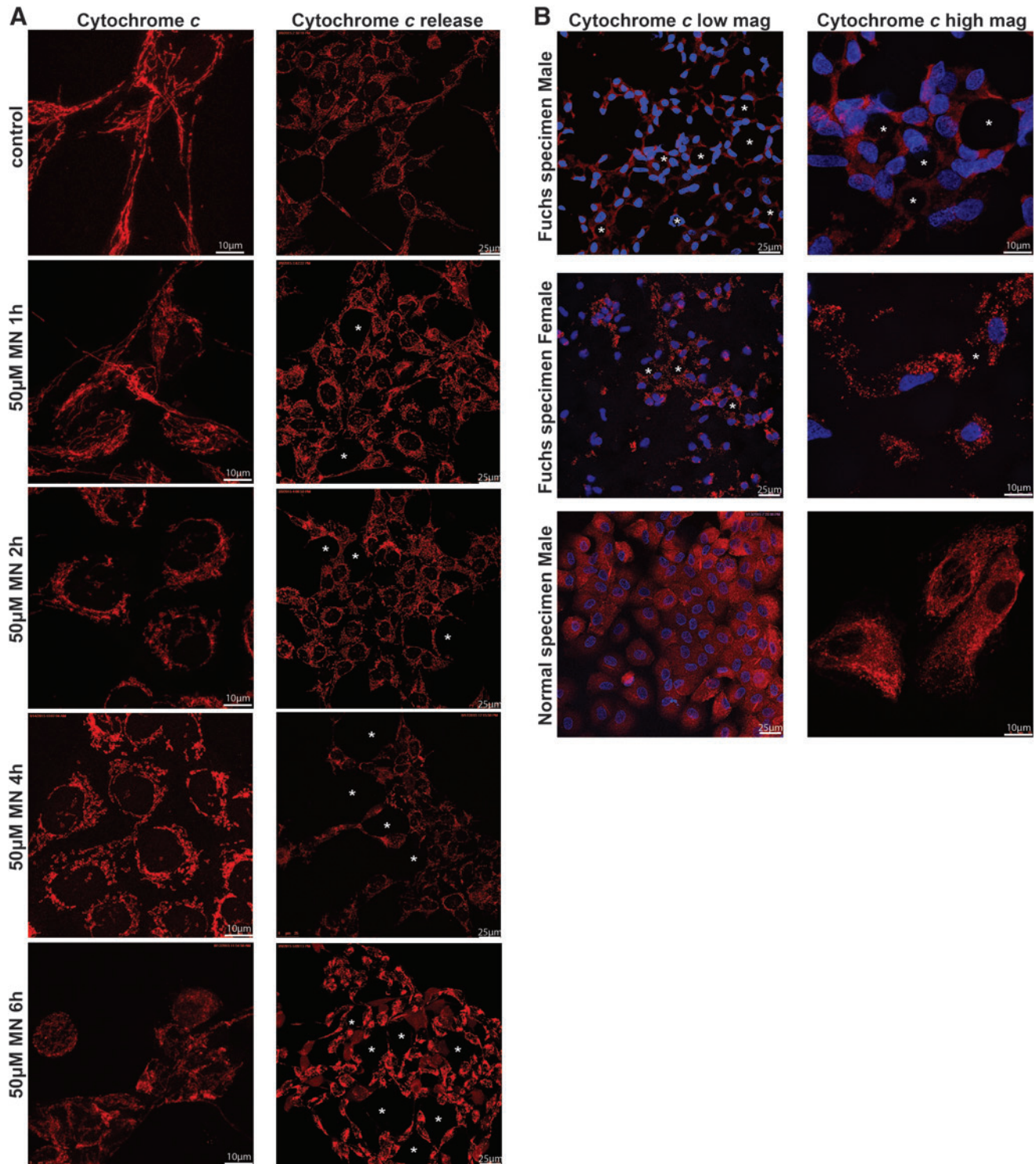
FIG. 4. MN treatment causes mitochondrial fragmentation in human corneal cells. HCEnC-21T cells were treated with 50 μM MN for 0, 1, 2, 4, and 6 h (*left panel*), fixed, and stained using anticytochrome *c* antibody and DAPI to reveal mitochondrial morphology and the nucleus, respectively. **(A,** *left panel***)** Transition from the typical tubular mitochondrial network of normal cells (control and 1 h MN) into vesicular punctiform mitochondria (2, 4, and 6 h 50 μM MN). **(A,** *right panel***)** Shows cytochrome *c* release after 50 μM MN treatment. **(B)** Mitochondrial morphology of two representative FECD donor specimens (61 male and 64 female) and representative normal donor specimen (59 male), labeled with cytochrome *c* (*red*) and DAPI (*blue*). Fragmented mitochondria **(B,** *lower image***)** and cytochrome c release were around guttae (*). Shown are representative images of at least three independent experiments. DAPI, 6′-diamidino-2-phenylindole. To see this illustration in color, the reader is referred to the web version of this article at www.liebertpub.com/ars

MN-induced apoptosis is caspase dependent during rosette formation

Cell loss in FECD has been shown to be mediated by apoptosis and specifically p53 (2, 6, 23). Next, we investigated whether caspase activation was involved in rosette formation, leading to endothelial cell loss. Caspase-9 has been associated with the release of cytochrome *c* from the mitochondrial intermembrane space to the cytosol. Moreover, MN has been shown to induce apoptosis defined by the release of cytochrome *c* and caspase-9 and caspase-3 activation in pancreatic acinar cells (14). Therefore, we aimed to determine if the release of cytochrome *c* resulted in the activation of caspase-9 and subsequently its downstream effector caspase, caspase-3, in our *in vitro* model. HCEnC-21T and HCECi cells were subject to a time-dependent analysis with 50 μM MN detected by Western blotting (Fig. 5A–C). STS served as a positive control of apoptosis. Cleaved caspase-9, 35 and 37 kDa, was detected at 1 h with increasing expression at 2 and 4 h in HCEnC-21T cells (Fig. 5A), while in HCECi cells, peak expression of cleaved caspase-9 was seen at 4 h (Fig. 5B). In FECDi cells, cleaved caspase-9 was already detected at baseline (Fig. 5C). Procaspase-9 did not vary with or without treatment in HCEnC-21T or HCECi cells; however, FECDi cells had slightly higher expression of procaspase-9 compared with normal cells. The release of cytochrome *c* into the cytoplasm is a critical component in caspase-9 activation and therefore subsequent caspase-3 activation. Increased expression of cleaved caspase-3, 17 and 19 kDa, was observed at 4 h in HCEnC-21T cells (Fig. 5A, lower blot), while caspase-3 cleavage was observed starting at 1 h in HCECi cells (Fig. 5B, lower blot). Interestingly, FECDi cells had higher cleaved caspase-3 expression at baseline (Fig. 5C), suggesting that FECDi cells are prone to cell death.

Discussion

Corneal endothelium is a postmitotic cell type, which is susceptible to oxidative macromolecular damage due to lifelong exposure to sunlight and robust metabolic activity controlling corneal deturgescence. This study provides the first line of evidence presenting accumulation of oxidative DNA damage in FECD endothelium that in turn leads to depletion of mtDNA, mitochondrial dysfunction, fragmentation, and subsequent induction of endothelial cell death. In this study, we modeled the rosette formation in FECD by inducing endogenous oxidative stress with MN to depict a temporal relationship in the sequence of pathogenic events. MN is specifically relevant to the study of FECD as it is metabolized by the reductive system found to be deficient in FECD. When MN is neutralized by 2-electron reduction by NAD(P)H quinone dehydrogenase 1 (NQO1), it forms a stable hydroquinone without abnormal ROS generation. In
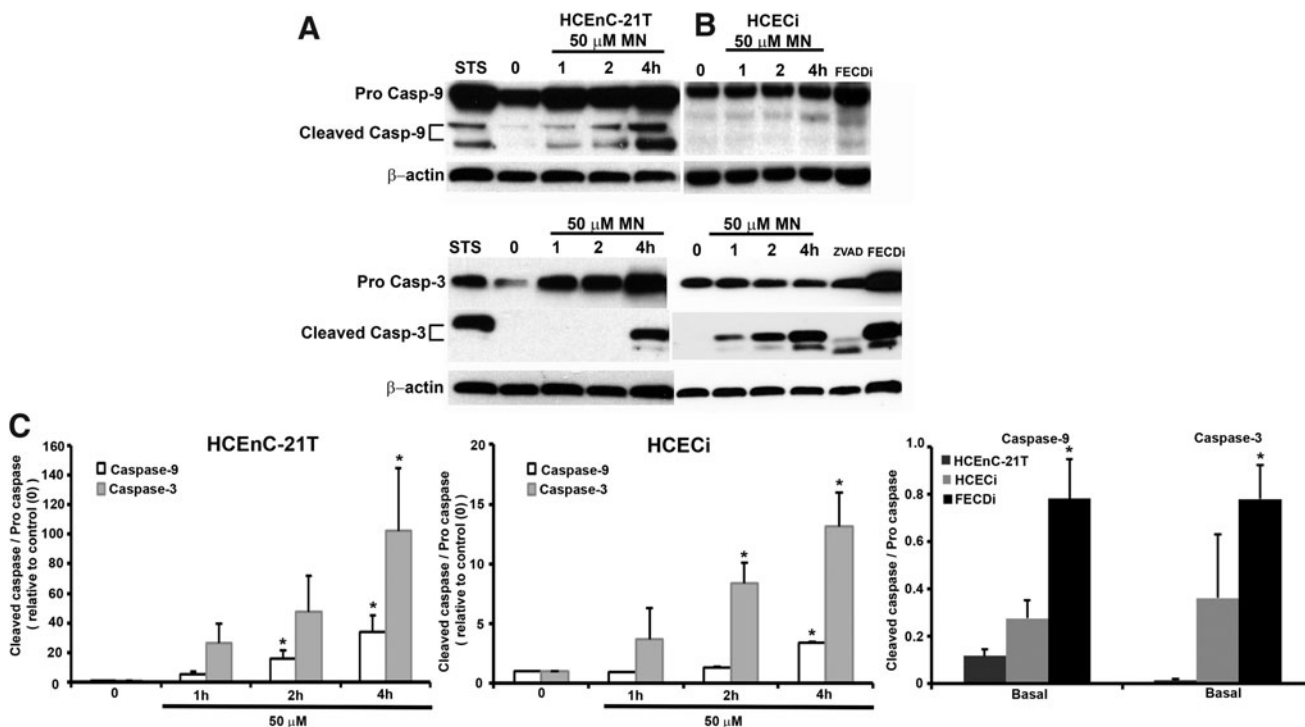
FIG. 5.   Caspase-9 and −3 activation in FECDi and MN-induced normal cells. HCEnC-21T and HCECi cells were exposed to 50 μM MN in a time-dependent manner. FECDi cells were untreated or in the basal state. Cells were collected and blotted for cleaved caspase-9 and cleaved caspase-3. Procaspase -9, total caspase-3, and β-actin were blotted for normalization and loading control. Bands represent **(A)** pro- and cleaved caspase-9 (*top*) and pro- and cleaved caspase-3 (*bottom*) in HCEnC-21T cells; **(B)** pro- and cleaved caspase-9 (*top*) and total and cleaved caspase-3 (*bottom*) in HCECi cells. Untreated FECDi cells display cleaved caspase-9 and caspase-3 activation. **(C)** Quantification of representative blots (*n* = 3). Data are expressed as the mean ± SE. Student's *t*-test was applied for statistical significance. *$p < 0.05$ from control (0) or *versus* normal cell line.

FECD, there is decrease in Nrf2-dependent antioxidant defense shown by decreased nuclear Nrf2 translocation and the ability to upregulate antioxidant response element-dependent antioxidants, such as NQO1 (2). Due to the deficient 2-electron reductive scavenging by NQO1, it is envisaged that MN is reduced by the 1-electron pathway, causing greater internal ROS production and overwhelming the antioxidant system that is dysfunctional in FECD (35). Treatment of HCEnCs with MN induced rosette formation, seen in FECD specimens, and decreased mitochondrial bioenergetic function such as ATP and MMP levels, leading to mitochondrial fragmentation and cytochrome c release, findings seen in FECD cells at baseline.

We show that HCEnCs in FECD accumulate DNA damage, which can be induced in normal endothelium with MN. The long-extension PCR technique was utilized to analyze genomic injury, rendering this to be the first study quantifying MN-induced DNA damage by LX-PCR. Previous studies have shown a dose-dependent increase in mtDNA damage in astrocytes upon exposure to 50, 75, and 100 μM MN for 1 h by Southern blot analysis. The break frequency was significantly higher in oligodendrocytes than astrocytes after 100 μM MN exposure (17). Interestingly, this type of assay did not detect any nDNA damage in neuronal cells after MN treatment. In contrast, our studies detected that MN induced both nDNA and mtDNA damage in the telomerase-immortalized HCEnCs after 50 μM. This difference between the studies could be attributed to the variability in the cell type response to MN and immortalization methods. In addition, qPCR has higher sensitivity in detecting DNA lesions than Southern blot analysis, which detects lesions per 50 kbs compared with per 10 kbs by qPCR. However, consistent with previous reports, our study found that MN-induced mtDNA lesion frequency was greater than that of nDNA in both cell lines, indicating that MN targets mtDNA more efficiently compared with nDNA (45). Interestingly, MN did not further increase DNA damage in FECDi. One of the possibilities is that the diseased cells have activated basal DNA repair, which was fairly effective in dealing with more stress once the cells were exposed to MN. More likely, FECDi cells have undergone more damage by MN and later died and thus were not captured by LX-PCR.

Our study detected that the central mechanism of HCEnC death in FECD, including that from MN, was increased generation of superoxide in mitochondria, loss of $\Delta\Psi$m, and depletion of ATP levels. Therefore, mtDNA damage likely has a significant contribution to the subsequent decline in mitochondrial physiology in FECD. Potential sources of mitochondrial dysfunction are superoxide-induced lipid peroxidation as well as inactivation of ETC due to decline in the mtDNA transcript levels (36, 45). Mitochondrial DNA encodes key protein components of the oxidative phosphorylation system involved in ATP production, lack of which leads to mitochondrial dysfunction. In support of this, we showed the correlation between loss of $\Delta\Psi$m and decline in ATP levels after exposure to 50 μM MN for 2 h, the dose at which mtDNA damage was induced in both normal HCEnC lines. Such DNA-damaging effects could be due to net damage being greater than repair mechanisms involved and possible loss of trafficking of nuclear encoded proteins from the cytosol to mitochondria due to loss of $\Delta\Psi$m, further potentiating the compromise of the repair activity in the mito-

chondria (39). Future studies should investigate further whether the damage seen in FECD is caused by the abnormal repair of nDNA and mtDNA in the diseased cells.

In normal HCEnCs, mitochondria form interconnected reticular networks that depend on mitochondrial fusion to maintain healthy mitochondrial morphology and function. In our study, loss of $\Delta\Psi$m led to mitochondrial fragmentation and inability to maintain the network, consistent with previous reports indicating the requirement of $\Delta\Psi$m to maintain healthy mitochondrial filamentous networks (18). Mitochondrial fragmentation was preceded by rosette formation and MN-induced DNA damage—the findings have not yet been conclusively correlated with mitochondrial fission in the past. There is a scarcity of evidence in the literature linking DNA damage with mitochondrial fission or lack of fusion. In contrast to our findings, DNA-damaging agents such as camptothecin caused mitochondrial fusion, not fission, in cortical neurons (44). Mitochondrial fusion was mediated by p53 activation, while p53-independent apoptotic stress, such as the one induced by STS, led to mitochondrial fragmentation. Apoptosis in FECD has been shown to be p53 dependent, but mitochondrial fission, and not fusion, was present in $ex\ vivo$ specimens and the MN stress model (2). Similarly, oxidative insult due to H_2O_2 was shown to induce changes in mitochondrial morphology (19, 20). Our study indicates that during rosette formation, DNA damage and depletion of ATP along with the fall in $\Delta\Psi$m likely lead to unbalanced fission and potential activation of autophagy/mitophagy, explaining the findings of markedly decreased mtDNA copy number in FECD endothelial specimens and cells. In support of this, induction of mitochondrial fragmentation with Phen, a DNA-damaging agent, leads to a decline in the mitochondrial DNA content and loss of mitochondrial mass in HeLa cells (33). Similarly to the findings in FECD specimens, a low content of mtDNA has been detected in the cerebrospinal fluid of Alzheimer's disease patients and has been postulated to be a causal factor for mitochondrial-driven neurodegenerative processes (34).

The biological consequence of mitochondrial dysfunction and fission in FECD is cell death (11, 28). We demonstrated that intracellular oxidative stress led to cytochrome c release and cleavage of caspase-9 and caspase-3 in HCENC-21T cells. Interestingly, FECDi demonstrated cleaved caspase-9 and caspase-3 bands without MN treatment, indicating activation of the apoptotic pathways at baseline. Similarly, MN induced caspase activation in MCF-9 cells, in cortical neurons, and pancreatic cells (1, 14, 40). Moreover, MN induced mtDNA damage, followed by cytochrome c release and caspase-dependent cell death in oligodendrocytes and microglia, with 100 μM MN treatment for 3 h, but did not cause significant cytochrome c release and caspase activation due to efficiently repaired mtDNA damage in astrocytes (17). However, another study has shown that MN-induced mitochondrial ROS causes mitochondrial dysfunction and cellular ATP depletion, but leads to caspase-independent cell death in mouse hippocampal neurons (12). Inability to activate caspases was attributed to MN-induced depletion of intracellular ATP levels, which are required for apoptosome formation. Our study detected a reduction in ATP levels after 1 h of 50 μM MN treatment, but ATP stores were most likely not depleted, fully allowing parallel caspase activation seen in FECD.

In summary, a temporal link between oxidative DNA damage and mitochondrial fission during rosette formation provides

novel insight into the general mechanisms of mitochondrial response to genotoxic stress. These studies turn our focus on the development of novel cytoprotective and antiaging therapies as potential options for treatment of mitochondrial dysfunction in FECD and other oxidative stress disorders.

Materials and Methods

Cell culture

Normal and FECD human corneal endothelial cell lines (HCECi and FECDi,), immortalized by infection of amphotropic recombinant retrovirus containing human papillomavirus type 16 genes E6 and E7, were gifts from Dr. May Griffith (Ottawa Hospital Research Institute, Ottawa, Ontario, Canada) and Dr. Rajiv R. Mohan (University of Missouri Health System, Columbia, MO) (15, 16). HCEnC-21T cells were immortalized by retrovirus transfection containing pBABE-puro-hTERT (38).

Human tissue

This study was conducted according to the tenets of the Declaration of Helsinki and approved by the Massachusetts Eye and Ear Institutional Review Board. Written and informed consent was obtained from patients undergoing surgical treatment for FECD. After surgical removal, the tissue was immediately placed in storage medium (Optisol-GS; Bausch & Lomb) at 4°C. Normal donor corneas ($n = 41$, age range 53–86) were purchased from National Disease Research Interchange or Tissue Banks International according to the criteria previously reported (21). FECD endothelium ($n = 48$) was derived from postkeratoplasty specimens (age range 47–82).

Cellular viability and morphology

HCEnC-21T, HCECi, and FECDi cells were plated as previously described (2). Cells were incubated with 1, 10, 25, 50, and 100 μM MN (Sigma-Aldrich) in DMEM (Life Technologies) with or without pretreatment with NAC (5 mM; Sigma-Aldrich) for 1 h. The cell number and viability were measured using an automatic cell counter (Countess; Life Technologies) and trypan blue dye exclusion, respectively. Phase-contrast microscopy (Leica DM IL LED) was employed to detect cell morphology.

Detection of DNA damage using long-extension QPCR

Total genomic DNA was isolated from HCEnC, HCECi, FECDi, and corneal human specimens (31 FECD and 22 normal corneas for mtDNA and 11 FECD and 15 normal for nDNA) and LX-PCR was performed and analyzed as previously described (13, 26, 37, 44). Specific primers were used to amplify mtDNA and nDNA (26). Conditions for each primer set were empirically optimized to ensure that the assay was in the linear range. The thermocycler (Biorad T100; Biorad) program included an initial denaturation at 94°C for 30 s, 26 cycles for β-globin (16 and 14 cycles for large and small mitochondrial target) at 94°C for 30 s, annealing at 64°C for 30 s, and extension at 68°C for 13:30 min for β-globin (8:50 min for large mitochondrial target and 30 s for small mitochondrial target). DNA lesion frequencies were calculated as described (36). Two-way analysis of variance (ANOVA) was utilized for statistical analysis, with p-values corresponding to <0.05 (*) as significant.

Intracellular ATP levels

After determining cellular viability, cells were resuspended in 100 μl warm HBSS and transferred to a 96-well plate, and ATP content was determined with recombinant firefly luciferase and D-luciferin in all three cell lines (HCEnC-21T, HCECi, and FECDi) using a bioluminescence ATP Determination Assay Kit (Molecular Probes).

Detection of intracellular ΔΨm using JC-1 dye

Cells were cultured in 12-well plates and stained using JC-1 dye (Cayman Chemical) according to the manufacturer's instructions for 15 min at 37°C, followed by a readout at 488/535 nm excitation and 590 nm emission wavelengths to measure green and red fluorescence as readout of $\Delta\Psi$m.

Mitochondrial superoxide detection

MitoSOXTM Red (Molecular Probes) was used for detection of mitochondrial superoxide production. Cells were treated with MN and washed with HBSS. A 5 mM stock of MitoSOX was prepared according to the manufacturer's protocol and 2.5 μM MitoSOX was added to the cells for 15 min at 37°C in the dark. Cells were washed, trypsinized, and centrifuged at 1200 rpm for 5 min. The pellet was washed and centrifuged at 1200 rpm for 5 min and resuspended in HBSS, and fluorescence intensity was analyzed using FACSCalibur™ (BD Biosciences).

Immunofluorescence staining

HCEnC-21T cells were seeded on two-well chamber slides and treated with 50 μM MN for 1, 2, 4, and 6 h. Rotenone (1 μM; Sigma-Aldrich) for 2 h was used as a positive control. In addition, HCEnC-21T cells were pretreated with or without 50 μM of the pan-caspase inhibitor, zVAD-fmk (Peptide Institute, Inc.), followed by 50 μM MN treatment for 1, 2, 4, and 6 h. Cells were fixed using 4% paraformaldehyde for 20 min at room temperature, permeabilized for 20 min using 0.15% Triton-X in PBS, and blocked for 1 h in 10% BSA (w/v). Tissue of FECD and normal donors was fixed using 4% PFA for 20 min at room temperature (RT), permeabilized using 0.3% Triton-X in 10% normal goat serum for 1.5 h at RT, and blocked for 30 min with 10% BSA. Cytochrome c (BD Bioscience #556432,) or clusterin (Santa Cruz Biotechnology; sc-8354) primary antibody was used overnight at 4°C, followed by secondary Alexa546 or 488-conjugated antibody (Invitrogen) for 1–2 h at RT. For the negative control, only secondary antibody was used. Nuclei were stained with DAPI (Vectashield; H1000) and observed using confocal microscopy (Zeiss) with different magnifications (40x zoom 1.5 and zoom 4). Specimens of 5 FECD donors (62F, 64 F, 61 M, 74 F, 81 F) and 4 normal cornea donors (52 F, 59 M, 72 M, 74 M) were used.

Western blotting

Cells were lysed in RIPA buffer containing HALT protease and phosphatase inhibitors (Thermo Fisher Scientific) for 30 min on ice. Protein concentration was determined using the BCA assay (Thermo Fisher Scientific) and samples were loaded onto a 12% Bis-Tris gel for SDS-PAGE and electrophoresed, followed by blotting onto a polyvinylidene difluoride membrane (Millipore). The membrane was

blocked in 5% nonfat milk in PBS 0.1% Tween-20 (PBST) for 1 h and incubated overnight with primary antibody at 4°C. Primary antibodies (Cell Signaling) used were caspase-9 (#9502), cleaved caspase-9 (#9501), caspase-3 (#9665), cleaved caspase-3 (#9664), and β-actin (Sigma Aldrich). Blots were exposed to HRP-conjugated anti-mouse or -rabbit IgG (Jackson ImmunoResearch Laboratories, Inc.) for 1 h. The membrane was developed with chemiluminescent substrate (Thermo Fisher Scientific).

Real-time reverse transcription–polymerase chain reaction

Total RNA was extracted from HCEnC-21T cells using an RNeasy extraction kit (Qiagen), as previously described (5). cDNA was prepared using the iScript cDNA synthesis kit (Biorad). TaqMan primers and probes for *CLU* (hs00156548_m1) and *TGFBI* (hs00932747_m1) and *GAPDH* (hs99999905_m1) were obtained from Applied Biosystems. Real-time PCR reactions were set up in triplicate (Probe Fast master mix; Kapa Biosystems) using the comparative threshold cycle (CT) method with the ABI StepOne Plus qPCR instrument (Applied Biosystems). Results were the average relative expression of the different genes normalized to GAPDH.

Acknowledgment

Author Disclosure Statement

No competing financial interests exist.

References

1. Akiyoshi T, Matzno S, Sakai M, Okamura N, and Matsuyama K. The potential of vitamin K3 as an anticancer agent against breast cancer that acts via the mitochondria-related apoptotic pathway. *Cancer Chemother Pharmacol* 65: 143–150, 2009.
2. Azizi B, Ziaei A, Fuchsluger T, Schmedt T, Chen Y, and Jurkunas UV. p53-regulated increase in oxidative-stress—induced apoptosis in Fuchs endothelial corneal dystrophy: a native tissue model. *Invest Ophthalmol Vis Sci* 52: 9291–9297, 2011.
3. Bahn CF, Falls HF, Varley GA, Meyer RF, Edelhauser HF, and Bourne WM. Classification of corneal endothelial disorders based on neural crest origin. *Ophthalmology* 91: 558–563, 1984.
4. Benard G and Karbowski M. Mitochondrial fusion and division: regulation and role in cell viability. *Semin Cell Dev Biol* 20: 365–374, 2009.
5. Bitar MS, Liu C, Ziaei A, Chen Y, Schmedt T, and Jurkunas UV. Decline in DJ-1 and decreased nuclear translocation of Nrf2 in Fuchs endothelial corneal dystrophy. *Invest Ophthalmol Vis Sci* 53: 5806–5813, 2012.
6. Borderie VM, Baudrimont M, Vallee A, Ereau TL, Gray F, and Laroche L. Corneal endothelial cell apoptosis in patients with Fuchs' dystrophy. *Invest Ophthalmol Vis Sci* 41: 2501–2505, 2000.
7. Cleland MM, Norris KL, Karbowski M, Wang C, Suen DF, Jiao S, George NM, Luo X, Li Z, and Youle RJ. Bcl-2 family interaction with the mitochondrial morphogenesis machinery. *Cell Death Differ* 18: 235–247, 2011.
8. Druzhyna NM, Hollensworth SB, Kelley MR, Wilson GL, and Ledoux SP. Targeting human 8-oxoguanine glycosylase to mitochondria of oligodendrocytes protects against menadione-induced oxidative stress. *Glia* 42: 370–378, 2003.
9. Eye Bank Association America. *2013 Eye Banking Statistical Report*. Washington, DC: Eye Bank Association of America, 2014, pp. 1–114.
10. Fang L, Li J, Flammer J, and Neutzner A. MARCH5 inactivation supports mitochondrial function during neurodegenerative stress. *Front Cell Neurosci* 7: 176, 2013.
11. Frank S, Gaume B, Bergmann-Leitner ES, Leitner WW, Robert EG, Catez F, Smith CL, and Youle RJ. The role of dynamin-related protein 1, a mediator of mitochondrial fission, in apoptosis. *Dev Cell* 1: 515–525, 2001.
12. Fukui M, Choi HJ, and Zhu BT. Rapid generation of mitochondrial superoxide induces mitochondrion-dependent but caspase-independent cell death in hippocampal neuronal cells that morphologically resembles necroptosis. *Toxicol Appl Pharmacol* 262: 156–166, 2012.
13. Furda AM, Bess AS, Meyer JN, and Van Houten B. Analysis of DNA damage and repair in nuclear and mitochondrial DNA of animal cells using quantitative PCR. *Methods Mol Biol* 920: 111–132, 2012.
14. Gerasimenko JV, Gerasimenko OV, Palejwala A, Tepikin AV, Petersen OH, and Watson AJ. Menadione-induced apoptosis: roles of cytosolic Ca(2+) elevations and the mitochondrial permeability transition pore. *J Cell Sci* 115: 485–497, 2002.
15. Griffith M, Osborne R, Munger R, Xiong X, Doillon CJ, Laycock NL, Hakim M, Song Y, and Watsky MA. Functional human corneal equivalents constructed from cell lines. *Science* 286: 2169–2172, 1999.
16. He Y, Weng J, Li Q, Knauf HP, and Wilson SE. Fuchs' corneal endothelial cells transduced with the human papilloma virus E6/E7 oncogenes. *Exp Eye Res* 65: 135–142, 1997.
17. Hollensworth SB, Shen C, Sim JE, Spitz DR, Wilson GL, and LeDoux SP. Glial cell type-specific responses to menadione-induced oxidative stress. *Free Radic Biol Med* 28: 1161–1174, 2000.
18. Ishihara N, Jofuku A, Eura Y, and Mihara K. Regulation of mitochondrial morphology by membrane potential, and DRP1-dependent division and FZO1-dependent fusion reaction in mammalian cells. *Biochem Biophys Res Commun* 301: 891–898, 2003.
19. Jahani-Asl A, Cheung EC, Neuspiel M, MacLaurin JG, Fortin A, Park DS, McBride HM, and Slack RS. Mitofusin 2 protects cerebellar granule neurons against injury-induced cell death. *J Biol Chem* 282: 23788–23798, 2007.
20. Jendrach M, Mai S, Pohl S, Voth M, and Bereiter-Hahn J. Short- and long-term alterations of mitochondrial morphology, dynamics and mtDNA after transient oxidative stress. *Mitochondrion* 8: 293–304, 2008.
21. Joyce NC and Zhu CC. Human corneal endothelial cell proliferation: potential for use in regenerative medicine. *Cornea* 23: S8–S19, 2004.
22. Jurkunas UV, Bitar M, and Rawe I. Colocalization of increased transforming growth factor-beta-induced protein (TGFBIp) and Clusterin in Fuchs endothelial corneal dystrophy. *Invest Ophthalmol Vis Sci* 50: 1129–1136, 2009.
23. Jurkunas UV, Bitar MS, Funaki T, and Azizi B. Evidence of oxidative stress in the pathogenesis of fuchs endothelial corneal dystrophy. *Am J Pathol* 177: 2278–2289, 2010.
24. Jurkunas UV, Bitar MS, Rawe I, Harris DL, Colby K, and Joyce NC. Increased clusterin expression in Fuchs' endothelial dystrophy. *Invest Ophthalmol Vis Sci* 49: 2946–2955, 2008.
25. Jurkunas UV, Rawe I, Bitar MS, Zhu C, Harris DL, Colby K, and Joyce NC. Decreased expression of peroxiredoxins

in Fuchs' endothelial dystrophy. *Invest Ophthalmol Vis Sci* 49: 2956–2963, 2008.

26. Kovalenko OA and Santos JH. Analysis of oxidative damage by gene-specific quantitative PCR. In: *Current Protocols in Human Genetics/Editorial Board*, edited by Jonathan L. Haines, *et al*. Chapter 19: Unit 19. Hoboken, NJ: John Wiley and Sons, Inc., 1, 2009.

27. Krachmer JH, Purcell JJ, Jr., Young CW, and Bucher KD. Corneal endothelial dystrophy. A study of 64 families. *Arch Ophthalmol* 96: 2036–2039, 1978.

28. Lee YJ, Jeong SY, Karbowski M, Smith CL, and Youle RJ. Roles of the mammalian mitochondrial fission and fusion mediators Fis1, Drp1, and Opa1 in apoptosis. *Mol Biol Cell* 15: 5001–5011, 2004.

29. Liu C, Chen Y, Kochevar IE, and Jurkunas UV. Decreased DJ-1 leads to impaired Nrf2-regulated antioxidant defense and increased UV-A-induced apoptosis in corneal endothelial cells. *Invest Ophthalmol Vis Sci* 55: 5551–5560, 2014.

30. Loor G, Kondapalli J, Schriewer JM, Chandel NS, Vanden Hoek TL, and Schumacker PT. Menadione triggers cell death through ROS-dependent mechanisms involving PARP activation without requiring apoptosis. *Free Radic Biol Med* 49: 1925–1936, 2010.

31. Misaka T, Miyashita T, and Kubo Y. Primary structure of a dynamin-related mouse mitochondrial GTPase and its distribution in brain, subcellular localization, and effect on mitochondrial morphology. *J Biol Chem* 277: 15834–15842, 2002.

32. Musch DC, Niziol LM, Stein JD, Kamyar RM, and Sugar A. Prevalence of corneal dystrophies in the United States: estimates from claims data. *Invest Ophthalmol Vis Sci* 52: 6959–6963, 2011.

33. Park SJ, Shin JH, Kim ES, Jo YK, Kim JH, Hwang JJ, Kim JC, and Cho DH. Mitochondrial fragmentation caused by phenanthroline promotes mitophagy. *FEBS Lett* 586: 4303–4310, 2012.

34. Podlesniy P, Figueiro-Silva J, Llado A, Antonell A, Sanchez-Valle R, Alcolea D, Lleo A, Molinuevo JL, Serra N, and Trullas R. Low cerebrospinal fluid concentration of mitochondrial DNA in preclinical Alzheimer disease. *Ann Neurol* 74: 655–668, 2013.

35. Radjendirane V, Joseph P, Lee YH, Kimura S, Klein-Szanto AJ, Gonzalez FJ, and Jaiswal AK. Disruption of the DT diaphorase (NQO1) gene in mice leads to increased menadione toxicity. *J Biol Chem* 273: 7382–7389, 1998.

36. Santos JH, Hunakova L, Chen Y, Bortner C, and Van Houten B. Cell sorting experiments link persistent mitochondrial DNA damage with loss of mitochondrial membrane potential and apoptotic cell death. *J Biol Chem* 278: 1728–1734, 2003.

37. Santos JH, Mandavilli BS, and Van Houten B. Measuring oxidative mtDNA damage and repair using quantitative PCR. *Methods Mol Biol* 197: 159–176, 2002.

38. Schmedt T, Chen Y, Nguyen TT, Li S, Bonanno JA, and Jurkunas UV. Telomerase immortalization of human corneal endothelial cells yields functional hexagonal monolayers. *PLoS One* 7: e51427, 2012.

39. Suen DF, Norris KL, and Youle RJ. Mitochondrial dynamics and apoptosis. *Genes Dev* 22: 1577–1590, 2008.

40. Tripathy D and Grammas P. Acetaminophen inhibits neuronal inflammation and protects neurons from oxidative stress. *J Neuroinflammation* 6: 10, 2009.

41. Tuberville AW, Wood TO, and McLaughlin BJ. Cytochrome oxidase activity of Fuchs' endothelial dystrophy. *Curr Eye Res* 5: 939–947, 1986.

42. Twig G and Shirihai OS. The interplay between mitochondrial dynamics and mitophagy. *Antioxid Redox Signal* 14: 1939–1951, 2011.

43. Wallace DC. Mitochondrial genetics: a paradigm for aging and degenerative diseases? *Science* 256: 628–632, 1992.

44. Wang DB, Garden GA, Kinoshita C, Wyles C, Babazadeh N, Sopher B, Kinoshita Y, and Morrison RS. Declines in Drp1 and parkin expression underlie DNA damage-induced changes in mitochondrial length and neuronal death. *J Neurosci* 33: 1357–1365, 2013.

45. Yakes FM and Van Houten B. Mitochondrial DNA damage is more extensive and persists longer than nuclear DNA damage in human cells following oxidative stress. *Proc Natl Acad Sci U S A* 94: 514–519, 1997.

46. Zavala J, Lopez Jaime GR, Rodriguez Barrientos CA, and Valdez-Garcia J. Corneal endothelium: developmental strategies for regeneration. *Eye* 27: 579–588, 2013.

47. Zhang X, Igo RP, Jr., Fondran J, Mootha VV, Oliva M, Hammersmith K, Sugar A, Lass JH, and Iyengar SK. Association of smoking and other risk factors with Fuchs' endothelial corneal dystrophy severity and corneal thickness. *Invest Ophthalmol Vis Sci* 54: 5829–5835, 2013.

Address correspondence to:
Dr. Ula Jurkunas
Department of Ophthalmology
Schepens Eye Research Institute
Mass Eye and Ear Infirmary
Harvard Medical School
20 Staniford Street
Boston, MA 02114

E-mail: ula_jurkunas@meei.harvard.edu

Abbreviations Used

$\Delta\Psi$m = mitochondrial membrane potential (MMP)
8-OHdG = 8-hydroxy-2′-deoxyguanosine
ANOVA = analysis of variance
ATP = adenosine triphosphate
CLU = clusterin
cyt c = cytochrome c
DAPI = 6′-diamidino-2-phenylindole
ETC = electron transport chain
FECD = Fuchs endothelial corneal dystrophy
LX-QPCR = long-extension qPCR
MN = menadione
mtDNA = mitochondrial DNA
NAC = N-acetyl-cysteine
nDNA = nuclear DNA
NQO1 = NAD(P)H quinone dehydrogenase 1
ROS = reactive oxygen species
STS = staurosporine
TGFBI = transforming growth factor, beta-induced
zVAD-fmk = benzyloxycarbonyl-Val-Ala-DL-Asp(O-methyl)-fluoromethylketone